Available online at www.sciencedirect.com
ScienceDirect
Journal of Power Sources 158 (2006) 831–836
JOURNAL OF POWER SOURCES
www.elsevier.com/locate/jpowsour

Short communication

Synthesis and characterization of lead dioxide active material for lead-acid batteries

Julián Morales [a,*], Galia Petkova [b], Manuel Cruz [a], Alvaro Caballero [a]

[a] *Laboratorio de Química Inorgánica, Universidad de Córdoba, Facultad de Ciencias, Avda. San Alberto Magno s/n, 14004 Córdoba, Spain*
[b] *Institute of Electrochemistry and Energy Systems (IEES), Bulgarian Academy of Sciences, Bulgaria*

Available online 3 February 2006

Abstract

Lead dioxide obtained by using various methods in combination with particles ranging from nanometric to micrometric size was tested as positive active material in lead-acid cells. The structural and textural properties of the material were determined by using X-ray photoelectron spectroscopy (XPS), X-ray diffraction (XRD), transmission and scanning electron microscopy (TEM and SEM), N_2 adsorption measurements and thermogravimetric analysis (TGA). Thin lead dioxide positive electrodes were prepared with obtained materials by spray deposition technique and were subjected to cycling tests. The combination of a small particle size (in the nanometric range) and the presence of water strongly bound to the lattice is essential to ensure a high utilization of the active material and good cycling properties of the positive electrode. Therefore, appropriate nanometric materials provide an effective method for increasing the efficiency of the active material in lead-acid batteries.

Keywords: Chemically prepared PbO_2; Thin electrodes; Lead-acid batteries

1. Introduction

Lead dioxide is the key component of the positive plate of a lead-acid battery; its textural and structural properties influence battery performance. The electrochemical activity of chemically prepared PbO_2 is known to be considerably lower than that of PbO_2 obtained by electrochemical reaction. Various factors such as hydrogen content, the presence of OH^- groups, oxygen vacancies and amorphous domains have been suggested as the origin of the differences [1–10]. Moseley and Bridger [11] demonstrated that chemically prepared PbO_2 mixed with PTFE can be used to obtain electrochemical capacity and suggested that the microstructure is the key for higher utilization and longer life of chemical PbO_2 electrodes.

One way to increase the reactivity of materials is the reduction of their particle size. In this context, nanometric materials provide substantially improved energy efficiency generation by virtue of their unique electronic and chemical properties and of the large area of their particles [12]. Recently, we found that nanostructured PbO_2 obtained by hydrolysis of Pb(IV) acetate delivers 65% of the theoretical capacity on prolonged cycling at a 1*C* discharge current [13]. In this work, we compared the electrochemical properties of PbO_2 obtained by following various synthetic procedures and in variable particle size. The best electrochemical response was obtained with highly hydrated PbO_2 consisting of particles in the nanometric range.

2. Experimental

We examined four different samples of PbO_2 hereafter named A–D. Table 1 summarizes the methods of synthesis and the type of the PbO_2 samples. Sample A was obtained by hydrolysis of a $Pb(CH_3–COO)_4$ precursor and sample B by exposing sample A to a hydrothermal treatment in a Berghof high pressure autoclave at 175 °C for 4 days. Sample C was obtained from the positive plate of a commercial battery supplied by Exide, Tudor SA. Finally, sample D was commercially available PbO_2 supplied by Aldrich.

X-ray diffraction (XRD) patterns were recorded on a Siemens D-5000 diffractometer using Cu Kα radiation and a graphite monochromator. X-ray photoelectron spectra (XPS) were obtained on a Physical Electronics PHI 5700 spectrometer using unmonochromated Mg Kα radiation as excitation source. The binding energy was calibrated with respect to the adventitious carbon C 1s line at 284.8 eV. Scanning electron microscopy

* Corresponding author. Tel.: +34 957218620; fax: +34 957218621.
E-mail address: iq1mopaj@uco.es (J. Morales).

0378-7753/$ – see front matter © 2005 Elsevier B.V. All rights reserved.
doi:10.1016/j.jpowsour.2005.11.021

Table 1
Method of synthesis of the PbO_2 samples, crystallite size, surface area, pore volume and diameter, and weight loss obtained from the TG curves

Sample	Synthetic method	Type	Crystallite size [nm]	S_{BET} [$m^2\,g^{-1}$]	V_p [$ml\,g^{-1}$]	D_p [nm]	Weight loss (%) (300 °C)
A	Hydrolysis of a $Pb(CH_3–COO)_4$ precursor	Nanostructured	7	32.7	0.192	21.5	3.5
B	Sample A with hydrothermal treatment at 175 °C for 4 days	Hydrothermal	38	18.3	0.098	23.4	1.0
C	Obtained from a positive plate of a commercial battery	PAM	42	6.6	0.061	36.6	0.8
D	Chemically synthesized	Aldrich	44	1.2	0.019	63.4	0.4

(SEM) images were obtained on a JEOL 6400 microscope. Transmission electron microscopy (TEM) was performed with a Philips CM-10 instrument. BET surface areas were determined from N_2 adsorption measurements made with a Micromeritics ASAP 2000 system. Thermogravimetric curves were recorded on a Cahn 2000 thermobalance under air atmosphere.

Electrochemical tests were performed by using small conventional lead-acid cells consisting of one positive and two negative electrodes. Positive electrodes, 1 cm^2 in size, were prepared by spraying an aqueous suspension of active material over both sides of lead alloy sheets (Pb–1.14% Sn–0.03% Ca, 0.3 mm thickness) according to a procedure described elsewhere [14]. All electrochemical measurements and cycling tests were carried out by using either a Solartron 1470A or an Arbin BT 2000 battery test system in a 1.28 s.g. H_2SO_4 solution at 25 °C. A $Hg/Hg_2SO_4/H_2SO_4$ (s.g. 1.28) reference electrode was used and all potential values given referred to this electrode.

3. Results and discussion

3.1. Sample characterization

Fig. 1 shows the XRD spectra for the samples. All patterns were indexed in a tetragonal system and cell dimensions were consistent with β-PbO_2. Although no significant differences in lattice parameters were observed, changes in peak intensity and width were clearly detected. The average crystallite size was calculated from the full width at the half maximum (FWHM) of [1 1 0] diffraction lines using the Scherrer equation. The data thus obtained are shown in Table 1. Sample A exhibited the lowest crystallite size. The hydrothermal treatment clearly increased crystallite size to a calculated value similar to those of samples C and D.

Fig. 2 shows the N_2 adsorption/desorption isotherms. The shape of the isotherm for sample A is between those of types II and IV in the BDDT classification [15], with a hysteresis loop associated to capillary condensation in a mesoporous system. The shape of the isotherms for samples C and D is closer to type II, which corresponds to non-porous or macroporous solids; the origin of the small hysteresis loop observed for electrochemically obtained PbO_2 must be the interparticle space arising from particle agglomeration. The isotherm shape of sample B is more similar to that of sample A, albeit with less marked hysteresis. The BET surface areas and the average pore volumes and diameters, calculated by using the Barret–Joyner–Halendar method [16], are shown in Table 1. Sample A, with the lowest crystallite size, had the highest surface area and pore volume, and the lowest pore size. By contrast, samples C and D, with narrow XRD peaks and high crystallite sizes, had a low BET surface area (especially commercial PbO_2, the pore size of which is typical of macroporous materials). The surface area of sample B is in between those of samples A and C, with a pore size somewhat higher but a pore volume substantially lower than that of sample A.

The particles of sample A tended to agglomerate and adopt a round shape as can be observed from SEM image (Fig. 3a). TEM analysis (Fig. 4a) revealed a morphology consisting of rather homogeneous PbO_2 nanoparticles ranging from 15 to 20 nm in size. HREM exposed the crystalline nature of the PbO_2 nanoparticles (Fig. 4b). The interplanar spacing was calculated to ca. 3.50 Å, which corresponds to the orientation of (1 1 0) atomic planes. On the other hand, commercial PbO_2 (sample D) consists of larger, less uniform *pseudo*-polyhedral particles with

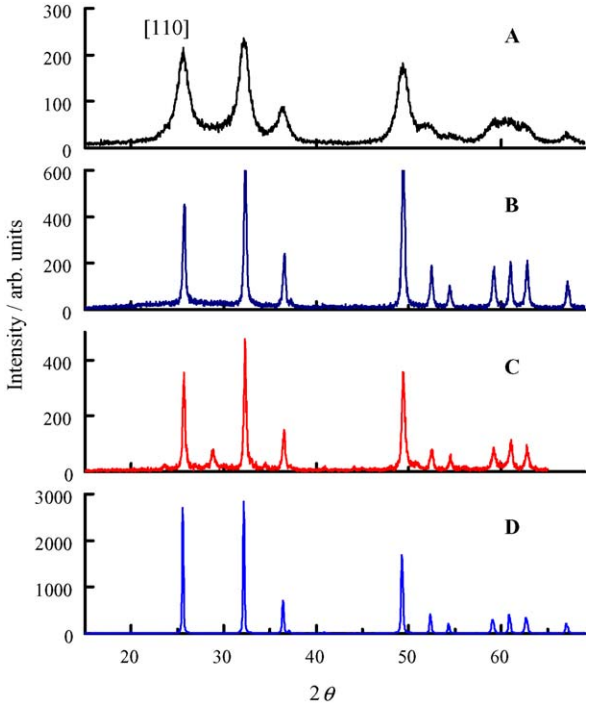

Fig. 1. (A–D) XRD patterns for the PbO_2 samples.

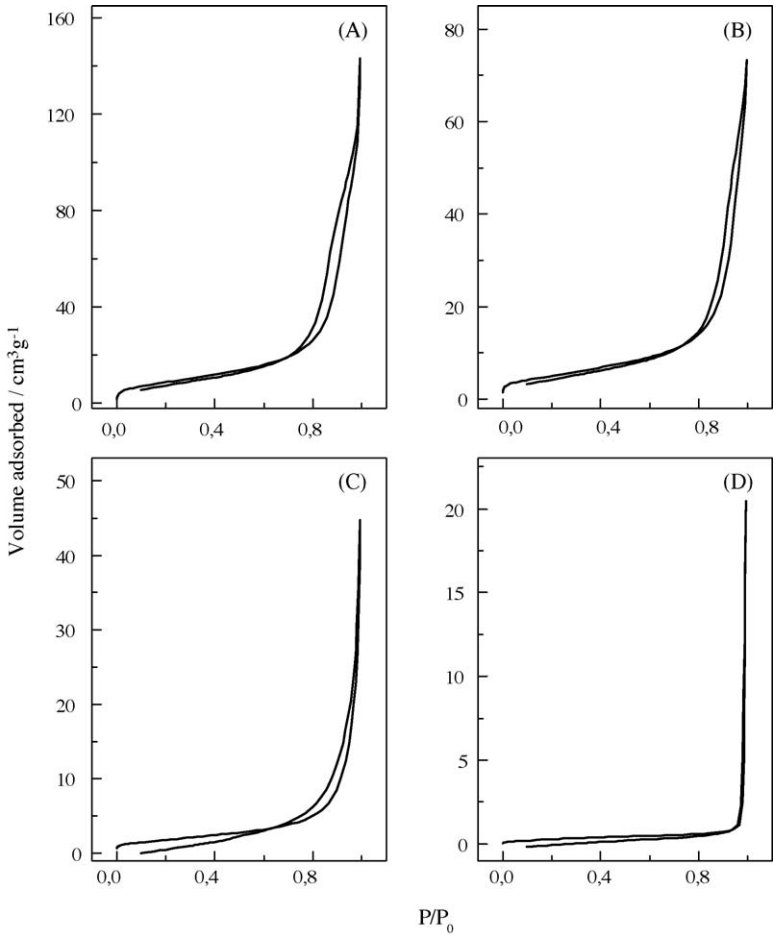

Fig. 2. (A–D) N_2 adsorption/desorption isotherms for the PbO_2 samples.

well-defined edges and vertices (Fig. 3d). The particle sizes of samples B and C (Fig. 3b and c) are in between those of the other two samples, which is consistent with their specific surface areas. In fact, the sample B that possesses a higher specific surface also has a lower particle size.

The tetravalent state of lead in all samples was confirmed from XPS data. The Pb 4f spectra for all samples exhibited two well-defined, symmetric peaks centred at 137.7 and 142.6 eV and corresponding to $4f_{7/2}$ and $4f_{5/2}$, respectively, consistent with the spectral values for PbO_2 [17,18]. Table 2 shows the binding energies (BE) of the two peaks. The constancy of BE and FWHM suggests that the chemical environment of Pb barely changes with the synthetic procedure. The largest differences were observed in the O 1s signal, which was deconvoluted in two components at 529.1 and 530.8 eV (Fig. 5). The binding energies and relative peak area of the two components are given in Table 2. The peak at 529.1 eV can be assigned to the oxygen atoms directly bound to Pb. The oxygen at 530.8 eV is probably due to adsorbed OH^- groups and/or water molecules.

Table 2
Data for binding energies (eV) of the Pb 4f and O 1s peaks for the PbO_2 samples

Sample	Pb $4f_{7/2}$	Pb $4f_{5/2}$	O 1s
A	137.7 (1.33)[a]	142.6 (1.32)	529.5 [48.5][b] 530.8 [51.5]
B	137.6 (1.34)	142.6 (1.33)	529.1 [80.0] 530.8 [20.0]
C	137.7 (1.31)	142.6 (1.33)	529.2 [90.8] 530.9 [9.2]
D	137.7 (1.32)	142.6 (1.34)	529.2 [95.0] 530.8 [5.0]

[a] Full width at half maximum (FWHM).
[b] Relative peak area (%).

The results of the thermogravimetric analysis (TGA) of the samples are shown in Fig. 6. Sample A, consisting of nanometric PbO_2, exhibited a significant weight loss (ca. 3.5%) up to 300 °C; on the other hand, the other types of PbO_2 remained quite stable up to 350 °C. The weight loss is associated with the release of water, the content in which was well correlated with the intensity of the oxygen component at 530.8 eV (see Tables 1 and 2). Above 350 °C, a two-step weight loss was observed in all samples, the resulting product being identified as α-PbO. Again, sample A behaved differently, especially concerning the step associated with the decomposition of PbO_2 into Pb_3O_4. For sample A this reaction takes place between 350 and 450 °C. However, for the other samples oxygen is evolved above this range, thus demonstrating the greater instability of nanometric PbO_2.

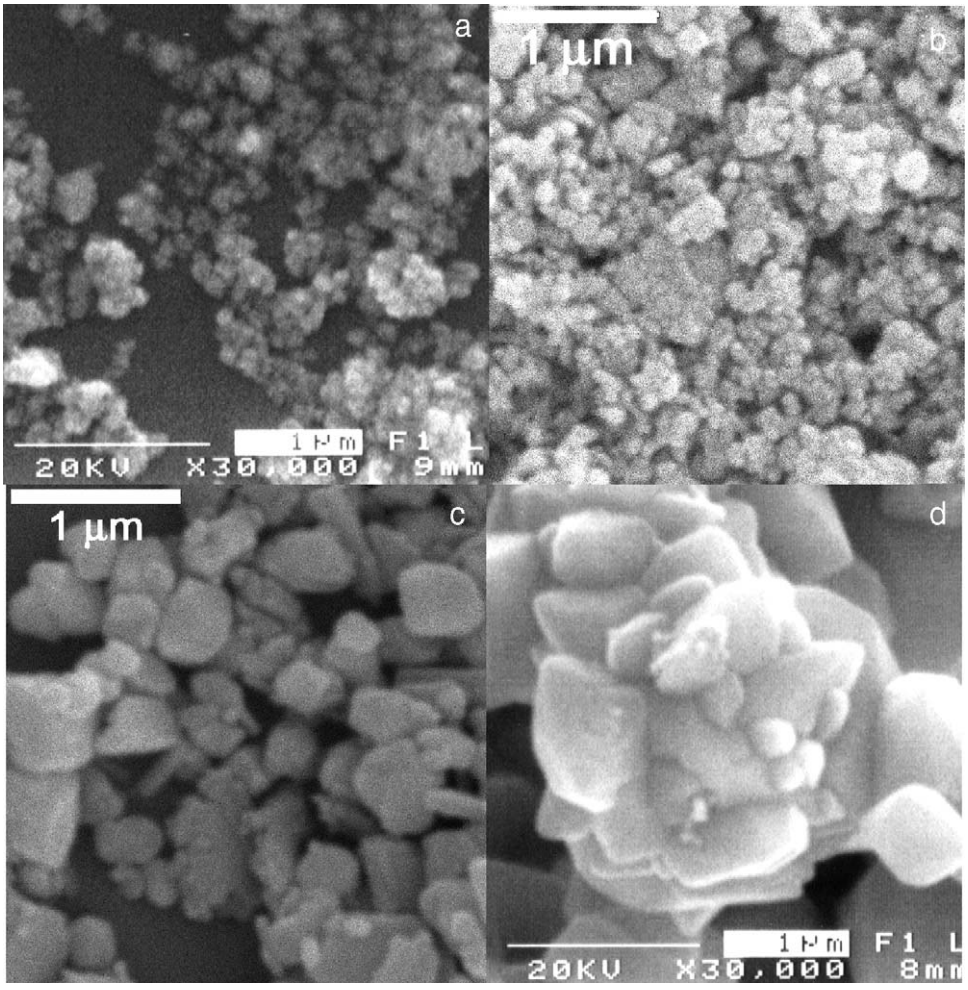

Fig. 3. (a–d) SEM micrographs of the PbO_2 samples.

All the results obtained revealed the singularity of sample A, the origin of which is probably due to its nanometric nature. On increasing particle size a tendency to a more pronounced similarity was observed both in the structural and textural properties and also in the thermal stability. The electrochemical properties of these samples were affected in a similar manner as shown below.

3.2. Electrochemical properties

The electrochemical performance of different types of PbO_2 was compared in charge/discharge tests with thin positive electrodes. Highly uniform deposits were prepared from a water suspension (5 g of PbO_2 in 50 ml of water, substrate temperature 140 °C) ranging from 10 mg cm^{-2}. Under these conditions,

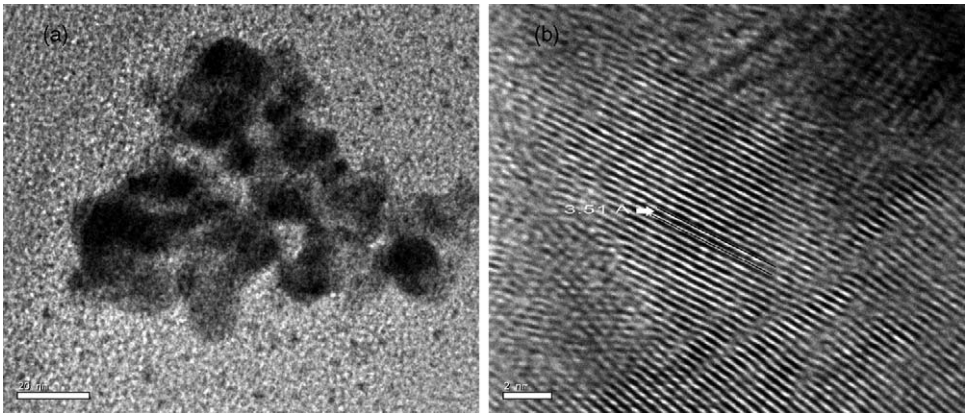

Fig. 4. TEM (a) and HRTM (b) images of sample A.

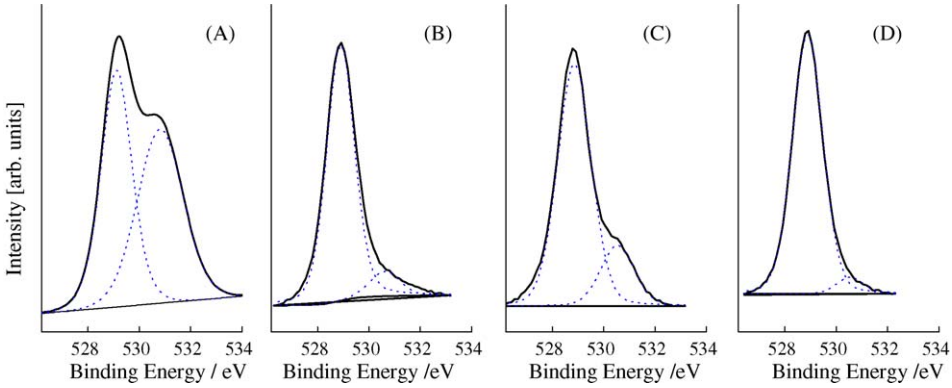

Fig. 5. (A–D) O 1s XPS peaks for the PbO_2 samples.

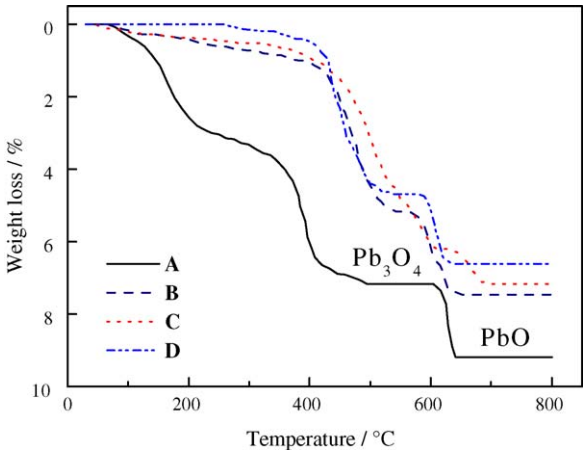

Fig. 6. TGA profiles for the PbO_2 samples.

the particles maintained both the PbO_2 structure and their main textural properties. In order to improve substrate/coating connection a preliminary charge up to $2C_t$ (C_t theoretical capacity) was applied for 6 h.

The cycle life performance of PbO_2 samples is illustrated in Fig. 7. The thin positive electrodes were discharged with a $1C$ discharge current to 0.7 V (corresponding to 100% DOD) and charged to an overcharge of 110% with the same charge current. The obtained behavior of the PbO_2 samples on cycling is consistent with the BET surface area and particle size data. The results confirm the well-known fact that the higher specific surface area is responsible for the increased capacity of the active material. Commercial PbO_2 (sample D) exhibited the worst response and the delivered capacity barely exceeds 40 mAh g^{-1}. Samples B and C behaved similarly after the 70th cycle. Thus, they delivered a capacity of about 120 mAh g^{-1}, which is 50% of the theoretical capacity. The difference in the capacity values of samples B and C at the initial stage of cycling can be ascribed to differences in the textural properties of both samples. The smaller surface area (Table 2) and the consequent greater particle size (Fig. 3) of sample C most likely result in decreased reactivity of the lead dioxide active material. The best electrochemical response was obtained from sample A, which consisted of nanometric particles. The nanostructured PbO_2 showed high utilization of the active material (about 75% of the theoretical capacity) and has the ability to deliver capacity in excess of 160 mAh g^{-1}. This electrode also showed the lowest Peukert coefficient ($n = 1.01$) (Fig. 8) compared with the other samples (1.05 and 1.09 for samples B and C, respectively), which indicates improved diffusion conditions and more effective electrochemical performance. The value of this coefficient for the three electrodes is notably lower than that reported for electrodes prepared by a conventional pasting procedure, 1.16 [19], thus suggesting that the thin films design enhances the diffusion prop-

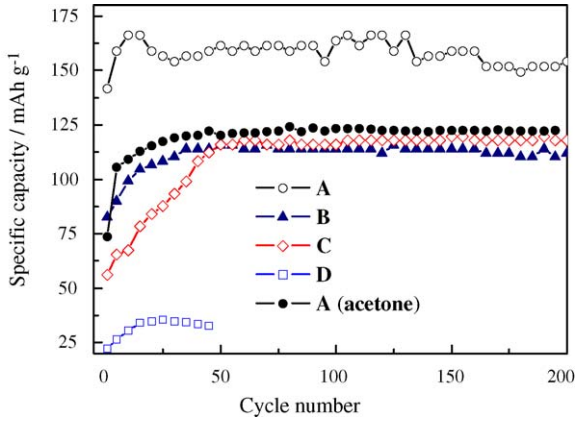

Fig. 7. Cycle life performance of the PbO_2 samples.

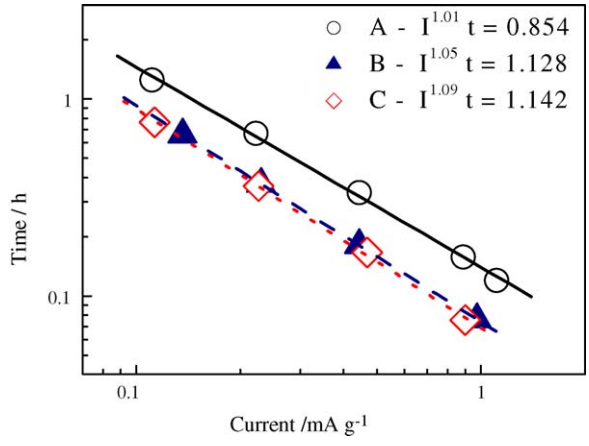

Fig. 8. Peukert dependence for the PbO_2 samples.

erties of the chemical species involved in the electrochemical reaction.

Good correlation was also observed between the discharge capacity and the weight loss at 300 °C, ascribed to structural water (see Table 2). As the water content increased, the delivered capacity also increased. The role of structural water in the reactivity of the positive active material has been emphasized by some authors [4,8,9,20,21]. In order to examine the effect of water on the electrochemical behavior of lead dioxide, the nanostructured PbO_2 material (sample A) was heated at 250 °C for 2 h to remove structural water. To avoid rehydration of nanometric particles, the thin positive electrode was prepared by suspending the PbO_2 material in acetone at a constant temperature of 80 °C. On cycling (Fig. 7) this electrode yielded a capacity similar to that obtained with the hydrothermally treated nanostructured PbO_2 (sample B), which possessed a higher particle size and a lower water content. The thermal treatment reduced the discharge capacity from 160 to 120 mAh g^{-1}, which provides indirect evidence for the influence of structural water on the electrochemical properties of PAM in lead-acid batteries. However, an unresolved question remains: the specific role of the active material/substrate connection, which must differ in both systems by effect of the different suspension media and deposition temperatures used.

The electrochemical activity of nanometric PbO_2 obtained by us exceeds that reported in Ref. [11]. Differences in particle size and/or in the plate design could account for the improved utilization. Other properties like the non-crystalline component in the material, that may play a significant role on the electrochemical activity as suggested by Hill [3], should not to be ruled out. For this reason, additional textural and structural studies intended to clarify this uncommon electrochemical activity are currently in progress.

4. Conclusions

Thin electrodes made from lead dioxide of variable BET surface area and particle size were tested as positive electrodes in lead-acid cells. The delivered capacity was found to be strongly dependent on both particle size and the water content of the particles. Large, well-crystallized particles, the water content of which is usually very low, provided poor electrochemical activity. On the other hand, nanometric PbO_2 in particle sizes from 15 to 20 nm yielded the best electrochemical response. This nanostructured electrode exhibits high utilization of the active material (about 65% of the theoretical capacity on discharge with 1*C* discharge current). The nanometric particle size, the large surface area of the PbO_2 material and the thin film design of the electrode are probably three key factors for the improved electrochemical activity of the positive active material.

Acknowledgements

This work was funded by the EU through contract ENK6-CT-2000-00078 and Junta de Andalucía (Group FQM-175).

References

[1] S.M. Caulder, J.S. Murday, A.C. Simon, J. Electrochem. Soc. 120 (1973) 1515.
[2] S.M. Caulder, A.C. Simon, J. Electrochem. Soc. 121 (1974) 1546.
[3] R.H. Hill, Mater. Res. Bull. 17 (1982) 769.
[4] R.J. Hill, M.R. Houchin, Electrochim. Acta 30 (1985) 559.
[5] A. Santoro, A. Caulder, S.M. Calder, J. Electrochem. Soc. 130 (1983) 1451.
[6] D. Pavlov, I. Balkanov, T. Halachev, P. Rachev, J. Electrochem. Soc. 136 (1989) 3189.
[7] D. Pavlov, J. Electrochem. Soc. 139 (1992) 3075.
[8] I. Petersson, E. Ahlberg, J. Power Sources 91 (2000) 137.
[9] N.J. Makalick, J. Electrochem. Soc. 122 (1975) 19.
[10] M. Dimitrov, D. Pavlov, J. Power Sources 93 (2001) 234.
[11] P.T. Moseley, N.J. Bridger, J. Electrochem. Soc. 131 (1984) 608.
[12] H. Huang, S.C. Yin, T. Kerr, N. Taylor, L.F. Nazar, Adv. Mater. 14 (2002) 1525.
[13] J. Morales, G. Petkova, M. Cruz, A. Caballero, Electrochem. Solid State Lett. 7 (2004) A75.
[14] A. Caballero, M. Cruz, L. Hernán, J. Morales, L. Sánchez, J. Power Sources 113 (2003) 376.
[15] S. Brunauer, W.S. Deming, L.S. Deming, E. Teller, J. Am. Chem. Soc. 62 (1940) 1723.
[16] E.P. Barret, L.G. Joyner, P.P. Halenda, J. Am. Chem. Soc. 73 (1951) 373.
[17] J.A. Taylor, G.M. Lancaster, J.W. Rabalais, J. Electron Spectrosc. Relat. Phenom. 13 (1978) 435.
[18] A. Velichenko, R. Amadelli, E. Baranova, D. Girenko, F. Danilov, J. Electroanal. Chem. 527 (2002) 56.
[19] F. Trinidad, F. Sáez, J. Velenciano, J. Power Sources 95 (2001) 24.
[20] D. Pavlov, A. Kirchev, M. Stoycheva, B. Monahov, J. Power Sources 137 (2004) 288.
[21] R. Fitas, L. Zerroual, N. Chelali, B. Djellouli, J. Power Sources 64 (1997) 57.